Power Density and Temperature Distributions Produced by Interstitial Arrays of Sleeved-Slot Antennas for Hyperthermic Cancer Therapy

Stefano Pisa, *Member, IEEE*, Marta Cavagnaro, *Member, IEEE*, Emanuele Piuzzi, Paolo Bernardi, *Life Fellow, IEEE*, and James C. Lin, *Fellow, IEEE*

***Abstract*—A graded-mesh finite-difference time-domain (FDTD) code, together with an alternate-direction-implicit finite-difference (ADI-FD) solution of the bioheat equation, are used for studying arrays of sleeved-slot antennas imbedded in a brain-equivalent phantom. The FDTD code allows efficient and accurate modeling of the fine structure of each antenna and of a sufficiently wide surrounding region. The ADI-FD solution of the bioheat equation allows evaluation of transient and steady-state temperature distributions in the brain-equivalent phantom with acceptable computational costs. The solution of the dosimetric-thermal problem in the volume irradiated by the antenna array permits the assessment of dimensions of the region where the temperature increase is above 43 °C (the threshold for an effective hyperthermia treatment) as a function of the array input power. Arrays made of three identical antennas placed at the vertices of equilateral triangles of 10-, 15-, and 20-mm sides have been studied. The temperature of 43 °C is reached in approximately 3 min in a deep-seated tumor region, from 10 to 40 mm in diameter, by applying input power levels between 2–32 W.**

***Index Terms*—Alternate-direction-implicit (ADI) methods, bioheat equation, catheter antenna, finite-difference time-domain (FDTD) methods, microwave hyperthermia, power density distribution, sleeved-slot antenna, temperature distribution, 2450-MHz antenna.**

I. Introduction

MICROWAVE interstitial techniques are used to produce localized deposition of electromagnetic (EM) energy in hyperthermia treatments for a variety of tumor sizes and sites. These techniques are generally used in conjunction with radiotherapy and chemotherapy since the ability of ionizing radiation to kill the tumor cell, and the antitumor action of drugs, are enhanced by hyperthermia [1]–[6]. For example, a typical combined brachytherapy-hyperthermia treatment consists of a hyperthermia session followed by interstitial radiotherapy and by a further hyperthermia application. It is worth noting that, in this combined therapy, the antennas can be inserted in the tumor tissue by using the same catheters prepared for the insertion of radioactive seeds.

In hyperthermia applications, the catheter antennas must provide efficient power delivery, good impedance matching at the frequency of operation, and a uniform specific absorption rate (SAR) distribution in the tumor region. However, if the region to be treated is large compared to the field penetration depth, the required SAR uniformity cannot be achieved with a single antenna, and the use of antenna arrays becomes necessary. The final goal of microwave therapy in the case of brain tumors is to produce temperatures in excess of 43 °C in the target tissue in order to guarantee the destruction of the tumor cells, while maintaining the temperature in the healthy tissues below 42 °C to avoid thermal damages.

The behavior of a center-driven dipole imbedded in a lossy medium has been studied in [7] and equations for the input impedance and for the electric field in the medium were derived. This theory has been used in [8] to investigate the effect of the dipole arm length on power deposition characteristics, showing that, for all the considered lengths, the SAR is sine shaped with the maximum occurring near the junction between the two arms, regardless of the insertion depth. The ability of multisection antennas in producing more uniform power distributions in the tissue has been demonstrated in [9]. These antennas are particularly suitable to treat superficial tumors that require a uniform power deposition along the antenna up to the skin surface. For deep-seated tumors, an applicator able to focalize the power in a region surrounding the distal end of the antenna and to prevent power flux along the feeding cable is instead necessary. To this end, sleeved-slot or cap-choke antennas, designed and studied for operation at 2450 and 915 MHz [10], [11], seem to be good candidates.

In order to increase the region of uniform SAR deposition, arrays of antennas have been studied both experimentally [12]–[14], by measuring the rate of temperature change caused by the radiated power, and theoretically, using approximate numerical procedures [12], [14], [15]. In particular, the approximate solution in [12] and [14] was based on the theory presented in [7], while a mixed semi-analytical/finite-difference time-domain (FDTD) approach was used in [15].

For an evaluation of the effectiveness of the microwave applicators, the dosimetric analysis must be integrated with the

Manuscript received April 17, 2003.

S. Pisa, M. Cavagnaro, E. Piuzzi, and P. Bernardi are with the Department of Electronic Engineering, University of Rome "La Sapienza," 00184 Rome, Italy (e-mail: pisa@die.uniromal.it).

J. C. Lin is with the Department of Bioengineering and the Department of Electrical and Computer Engineering, University of Illinois at Chicago, Chicago, IL 60607-7053 USA (e-mail: lin@ece.uic.edu).

Digital Object Identifier 10.1109/TMTT.2003.819214

thermal one to asses the region where the temperature is above the threshold for tumor-cell destruction and to estimate the required input power. Temperature distributions, produced by interstitial antennas in tumor tissues, have been experimentally evaluated by using microwave radiometry [14]. This approach allows the use of the same array both for irradiating the tissue and for reconstructing the induced heating patterns through radiometric measurements. Temperature distributions have been also computed by using explicit solutions of the bioheat equation [16], [17]. These solutions are accurate, but in the presence of conductors, and fine-resolution computational volumes, require small time steps to be stable and, hence, very long computation times to reach steady state. The time-step constraint is not present in implicit solutions [18], but they require the inversion of a sparse matrix with huge computational costs when the domain dimensions increase. This problem can be overcome by using an alternate-direction-implicit (ADI) approach that confines the problem solution to the inversion of three tri-diagonal matrices that can be performed very efficiently. However, in the past, ADI approaches have been used only for studying two-dimensional interstitial antenna arrays [19].

In this paper, a graded-mesh FDTD code, together with a three-dimensional (3-D) alternate-direction-implicit finite-difference (ADI-FD) solution of the bioheat equation, are used to study arrays of sleeved-slot antennas imbedded in a brain-equivalent phantom. The FDTD code allows the consideration of the antenna fine structure and of the mutual interaction among antennas. The ADI-FD solution of the bioheat equation allows the evaluation of transient and steady-state temperature distributions with a fine resolution in a brain-equivalent phantom.

II. Numerical Solution of the EM Problem

A previously developed 3-D graded-mesh FDTD code [20] has been improved in order to deal with multiple fine regions. In this manner, both a single and an array of sleeved-slot antennas have been studied. In the implemented code, the graded mesh is generated along the three Cartesian directions independently. Considering a given axis, a small spatial step is used in the region where the antenna is located. Starting from this region, the spatial step is multiplied successively by a constant factor (geometric series) up to the largest spatial step. This procedure is repeated wherever an antenna is located. In the present study, the fine-region cells are $0.06 \times 0.06 \times 0.12$ mm wide while the largest cell size employed is $0.6 \times 0.6 \times 0.6$ mm. In this way, the real array geometry is modeled with an adequate number of computational cells, but with limited memory occupation.

The considered sleeved-slot antenna was proposed in [10] for operation at 2450 MHz. The antenna is mounted on a UT-34 coaxial cable that is used for power delivery to the antenna. In Fig. 1(a), a longitudinal section of the antenna is depicted, while Fig. 1(b) reports a horizontal section in correspondence with the AA' plane of Fig. 1(a). Since for the proposed staircase structure of the coaxial cable the field distribution for the TEM mode is not analytically available, it was obtained with a two-dimensional finite-difference solution of the Laplace equation [21]. This distribution was then used as the spatial excitation at the BB' section of Fig. 1(a) for each antenna, imposing

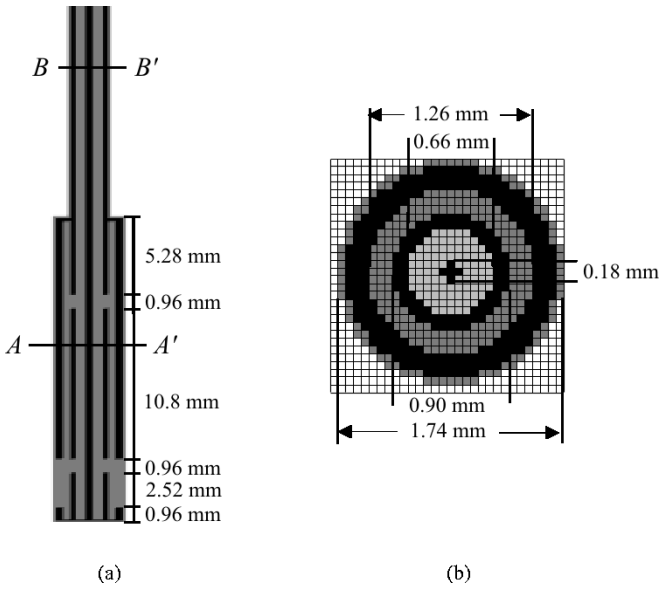

Fig. 1. (a) Longitudinal and (b) horizontal sections of the sleeved-slot antenna.

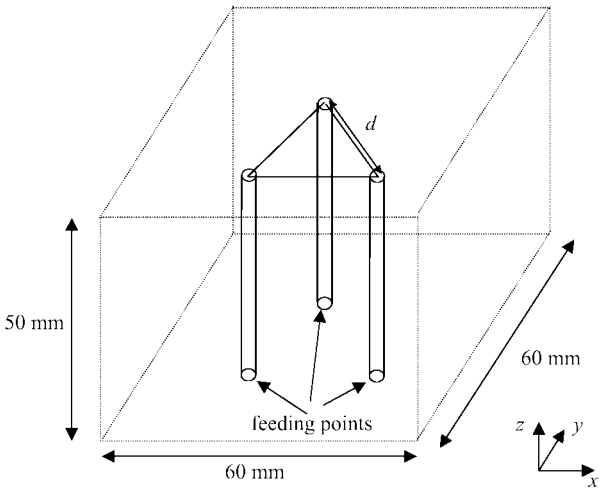

Fig. 2. Geometry of the triangular array in the $60 \times 60 \times 50$ mm phantom box.

a Gaussian-modulated sine-wave time behavior. This time behavior allows the study of the structure on a wide frequency range with a single FDTD run. Simulations are interrupted when the total energy in the studied domain is reduced by 30 dB, with reference to its maximum value. At this time, the antenna radiation impedances are evaluated as the ratio between the Fourier transforms of the voltage and the current at the feeds [BB' section in Fig. 1(a)].

The radiating structure was assumed to be inserted in a brain-tissue phantom ($\sigma = 1.23$ S/m, $\varepsilon_r = 33.5$) of dimension $60 \times 60 \times 50$ mm. The truncation of the computational domain was performed by using the uniaxial perfectly matched layer (UPML) absorbing boundary condition [22], [23]. Both a single antenna and triangular arrays have been studied by using the graded-mesh FDTD code. In particular, the triangular arrays were formed by locating the antennas at the vertices of three equilateral triangles whose sides are 10, 15, and 20 mm, respectively (Fig. 2).

Once the EM problem was solved by using the graded-mesh FDTD code with the Gaussian-modulated sine-wave excitation, the amplitude of each field component at 2450 MHz was obtained through a discrete Fourier transform of the time-domain field behaviors. Afterward, the SAR values at each cell (i,j,k) were evaluated as

$$\mathrm{SAR}(i,j,k)=\frac{\sigma(i,j,k)\left[\hat{E}_x^2(i,j,k)+\hat{E}_y^2(i,j,k)+\hat{E}_z^2(i,j,k)\right]}{2\rho(i,j,k)} \tag{1}$$

where $\sigma(i,j,k)$ and $\rho(i,j,k)$ are the conductivity and density of cell (i,j,k) and the amplitude of each field component was evaluated at the cell center as the average of the corresponding four field components placed at the cell edges.

It must be noted that, due to the graded mesh, the SAR values obtained refer to cells having different volumes and, in order for them to be used as input for the solution of the thermal problem, they have been uniformly sampled with a spatial step of 0.3 mm. This has been performed first dividing each cell into sub-cells of sides $0.06\times0.06\times0.06$ mm and then recombining $5\times5\times5$ of these sub-cells into the final ones of sides $0.3\times0.3\times0.3$ mm. These larger cells have been assigned a SAR value obtained by dividing the total power absorbed in the 125 sub-cells by the total mass.

III. Numerical Solution of the Thermal Problem

The temperature distribution $T=T(\boldsymbol{r},t)$ inside the brain-equivalent material has been obtained by using the bioheat equation (BHE) [24]

$$\nabla\cdot(K(\boldsymbol{r})\nabla T)+A(\boldsymbol{r})+Q_v(\boldsymbol{r})-B(\boldsymbol{r})(T-T_B) = C(\boldsymbol{r})\rho(\boldsymbol{r})\frac{\partial T}{\partial t}\left[\frac{W}{m^3}\right]. \tag{2}$$

The four terms on the left-hand side of (2) represent the heat transfer through internal conduction (K [W/(m · °C)] is the tissue thermal conductivity), metabolic heat production (A [W/m^3]), EM power deposition (Q_v [W/m^3]), and the heat exchange mechanism due to capillary blood perfusion proportional to the difference between blood and tissue temperature (T_B-T) through parameter B [W/(m^3 · °C)] linearly depending on blood flow. These terms are equated with the temperature increase (or decrease) per unit time multiplied by the thermal capacitance of 1 m^3 of tissue (right-hand side). The thermal capacitance is given by the product between the tissue specific heat (C [J/(kg · °C)]) and density (ρ [kg/m^3]).

The BHE must be solved with an appropriate boundary condition, capable of modeling the heat exchange between the phantom under study and the external environment. This boundary condition can be obtained by imposing the continuity of the heat flow perpendicular to the surface of the phantom, and can be expressed as [25]

$$-K(\boldsymbol{r})(\nabla T\cdot\boldsymbol{n}_0)_S=H(T_S-T_E)\left[\frac{W}{m^2}\right] \tag{3}$$

where S is the phantom surface, and $\boldsymbol{n}_0$ is the outward unit vector normal to S. The term on the right-hand side of (3) models heat losses due to convection and radiation, proportional to the difference between temperature of the phantom surface (T_S) and external temperature (T_E) through the parameter H [W/(m^2 · °C)].

To obtain a finite-difference formulation of the BHE (2), the body under consideration is divided into cubic cells of side δ, and the temperature is evaluated in a grid of points defined at the centers of the cells. Temperatures are computed at equally spaced time instants with a time step equal to δt. In the following, the expression $T^n(i,j,k)$ will be used to identify the temperature computed at time $n\ \delta t$ in the center of the cell (i,j,k).

The space derivatives of the BHE are of the second order and, therefore, a central-differencing scheme can be adopted for their approximation. The time derivative, instead, is of the first order and, therefore, either forward or backward differencing has to be used, resulting in explicit and implicit finite-difference schemes, respectively. In the implicit scheme, the temperature at a given point at the time $(n+1)\ \delta t$ depends on temperatures in neighboring points at the same time step. The implicit method, therefore, generally requires, for the computation of the temperature at a given time instant, the inversion of an $N\times N$ matrix, where N is the number of cells. This kind of procedure can result in huge computational costs. However, it has the great advantage of being unconditionally stable and, therefore, of allowing the use of arbitrarily large time steps (as opposed to explicit methods, which have a stability constraint).

The ADI-FD formulation adopted in this study is based on the observation that if the implicit formulation is applied to a mono-dimensional thermal problem, the resulting matrix is tri-diagonal and, therefore, the matrix inversion is computationally very efficient. Moreover, for mono-dimensional problems, an increased accuracy of the finite-difference solution can be obtained by computing temperatures at the time instant $(n+1/2)\ \delta t$, which corresponds to also using a central- difference scheme for the time derivative. The resulting scheme, known as the Crank–Nicolson (C–N) scheme [26], is still implicit and unconditionally stable. The ADI technique, originally developed by Peaceman and Rachford [27] and Douglas [28], is based on a reduction of the 3-D problem to a sequence of mono-dimensional C–N problems, which, as observed above, can be solved very efficiently. The procedure consists of using a sequence of approximate solutions of the equation ($T^*(i,j,k)$, $T^{**}(i,j,k)$, $T^{***}(i,j,k)$) with the third solution being finally used as the best approximation for the temperature at the next time step $T^{n+1}(i,j,k)$. The first approximate solution is obtained using a C–N approach for the time and space derivatives along the x-axis, while backward differencing is used for the y- and z-axes. The second approximate solution is then obtained extending the C–N approach to the y-axis, but using the first-step approximation for the x-axis derivative. Finally, the last approximate solution is derived using the C–N approach on the z-axis, while maintaining the first- and second-step approximations for the x- and y-axis derivatives, respectively.

Application of the ADI approach to the BHE yields the following set of tri-diagonal finite-difference equations for the three sub-steps:

$$\begin{aligned}
&- CO_{0IM}(i,j,k)T^{*}(i-1,j,k)\\
&- CO_{0IP}(i,j,k)T^{*}(i+1,j,k)\\
&+ \big(2 + CO_{0IM}(i,j,k) + CO_{0IP}(i,j,k)\\
&\quad + CO_2(i,j,k)\big)T^{*}(i,j,k)\\
&= CO_{0IM}(i,j,k)T^{n}(i-1,j,k)\\
&\quad + CO_{0IP}(i,j,k)T^{n}(i+1,j,k)\\
&\quad + 2CO_{0JM}(i,j,k)T^{n}(i,j-1,k)\\
&\quad + 2CO_{0JP}(i,j,k)T^{n}(i,j+1,k)\\
&\quad + 2CO_{0KM}(i,j,k)T^{n}(i,j,k-1)\\
&\quad + 2CO_{0KP}(i,j,k)T^{n}(i,j,k+1)\\
&\quad + \begin{pmatrix} 2 - CO_2(i,j,k) - CO_{0IM}(i,j,k)\\ -CO_{0IP}(i,j,k)\\ -2CO_{0JM}(i,j,k) - 2CO_{0JP}(i,j,k)\\ -2CO_{0KM}(i,j,k) - 2CO_{0KP}(i,j,k)\end{pmatrix} T^{n}(i,j,k)\\
&\quad + 2CO_3(i,j,k)(A + Q_v)\\
&\quad + 2CO_2(i,j,k)T_b
\end{aligned} \tag{4a}$$

$$\begin{aligned}
&- CO_{0JM}(i,j,k)T^{**}(i,j-1,k)\\
&- CO_{0JP}(i,j,k)T^{**}(i,j+1,k)\\
&+ \big(2 + CO_{0JM}(i,j,k) + CO_{0JP}(i,j,k)\\
&\quad + CO_2(i,j,k)\big)T^{**}(i,j,k)\\
&= -CO_{0JM}(i,j,k)T^{n}(i,j-1,k)\\
&\quad - CO_{0JP}(i,j,k)T^{n}(i,j+1,k)\\
&\quad + \big(CO_{0JM}(i,j,k) + CO_{0JP}(i,j,k)\big)T^{n}(i,j,k)\\
&\quad + \big(2 + CO_2(i,j,k)\big)T^{*}(i,j,k)
\end{aligned} \tag{4b}$$

$$\begin{aligned}
&- CO_{0KM}(i,j,k)T^{n+1}(i,j,k-1)\\
&- CO_{0KP}(i,j,k)T^{n+1}(i,j,k+1)\\
&+ \big(2 + CO_{0KM}(i,j,k) + CO_{0KP}(i,j,k)\\
&\quad + CO_2(i,j,k)\big)T^{n+1}(i,j,k)\\
&= -CO_{0KM}(i,j,k)T^{n}(i,j,k-1)\\
&\quad - CO_{0KP}(i,j,k)T^{n}(i,j,k+1)\\
&\quad + \big(CO_{0KM}(i,j,k) + CO_{0KP}(i,j,k)\big)T^{n}(i,j,k)\\
&\quad + \big(2 + CO_2(i,j,k)\big)T^{**}(i,j,k)
\end{aligned} \tag{4c}$$

where

$$CO_{0IM}(i,j,k) = \frac{2K(i-1,j,k)K(i,j,k)}{K(i-1,j,k) + K(i,j,k)} \times \frac{\delta t}{C(i,j,k)\rho(i,j,k)\delta^2}$$

the expressions for $CO_{0IP}(i,j,k)$, $CO_{0JM}(i,j,k)$, $CO_{0JP}(i,j,k)$, $CO_{0KM}(i,j,k)$, and $CO_{0KP}(i,j,k)$ can be directly derived from the definition of $CO_{0IM}(i,j,k)$

$$CO_2(i,j,k) = \frac{B(i,j,k)\delta t}{C(i,j,k)\rho(i,j,k)}$$

$$CO_3(i,j,k) = \frac{\delta t}{C(i,j,k)\rho(i,j,k)}.$$

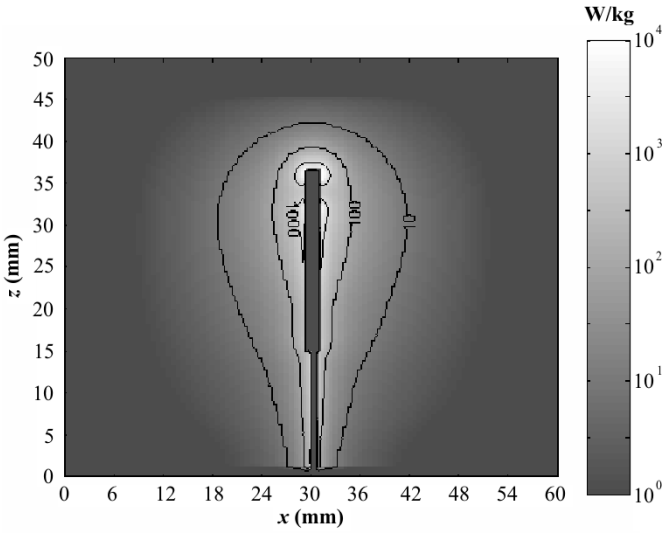

Fig. 3. Local SAR distribution for 1.0 W of radiated power in a vertical plane passing through the antenna axis.

In particular, the expressions for the CO_{0xx} coefficients take into account the effect of thermal nonhomogeneities in the phantom. In fact, if K_1 and K_2 are the thermal conductivities of two neighboring cells, heat flows through the series connection of two thermal conductances, equal to $K_1\delta^2/(\delta/2)$ and $K_2\delta^2/(\delta/2)$, respectively. Therefore, heat flow from the center of the first cell to the center of the second, through the boundary face, can be supposed to occur through an overall thermal conductance equal to $2K_1K_2\delta^2/(K_1+K_2)\delta$.

In case of boundary cells, with one or more faces affected by convective heat exchange with the external environment, a set of equations similar to (4) is used to take into account the boundary condition (3). These equations can be easily obtained introducing a fictitious external node used for the computation of the thermal gradient on the boundary surface.

IV. Results

SAR and temperature increment distributions of both a single antenna and an array of sleeved-slot antennas have been studied in order to assess their capability in heating tumor regions of varying dimensions.

For the single sleeved-slot antenna, imbedded in the brain-equivalent phantom, the computed radiation impedance results in a magnitude of the reflection coefficient at 2.45 GHz equal to 0.48 [29]. Fig. 3 shows, in logarithmic scale, the SAR distribution, obtained using the graded-mesh FDTD code, for a single sleeved-slot antenna radiating a power of 1.0 W inside a brain-equivalent phantom. The SAR distribution, referring to a vertical plane passing through the antenna axis, reveals, very close to the antenna surface, two regions of high SAR just above and below the first slot, placed 4 mm from the antenna tip. At increasing radial distances from the antenna surface, a pear-shaped behavior can be observed.

The computed SAR has then been used as the heating source, and the thermal problem has been solved by using the ADI solution of the bioheat equation. As the aim of the simulations

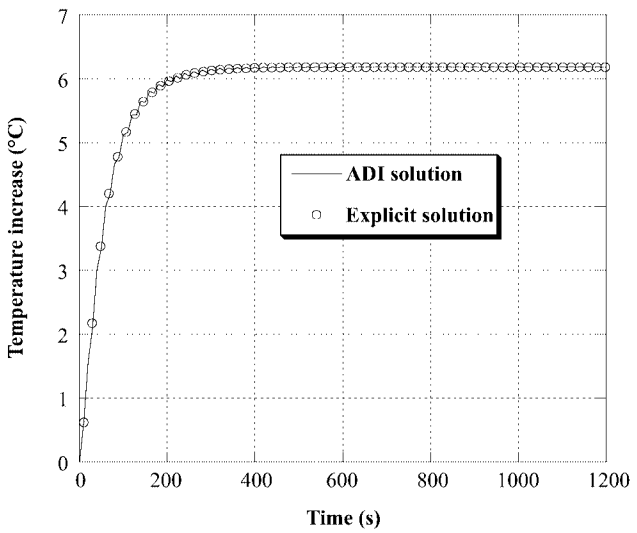

Fig. 4. Time behavior of the temperature increase. The results obtained by using ADI and explicit solutions are compared.

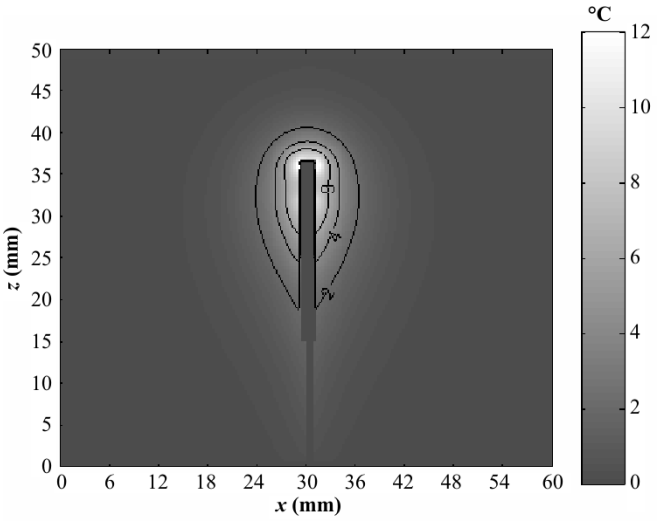

Fig. 5. Temperature distribution in the same plane of Fig. 3 for 1.0 W of radiated power.

was only to obtain temperature increments and not the absolute temperature values, the metabolic heat production has been neglected, and blood and external temperature have been assumed equal to 0 °C. In this way, the initial temperature is uniform and equal to 0 °C and, thanks to the BHE linearity, the steady-state value obtained after the microwave exposure is directly equal to the temperature increment. An adiabatic boundary condition ($H = 0$ W/(m^2 · °C)) has been assumed on the surface of the antennas, while a high convection coefficient ($H = 70$ W/(m^2 · °C)) has been assumed on the external phantom surface. The first condition derives from the assumption of a perfectly insulating catheter, while the second one is roughly equivalent to fixing the external surface temperature to 0 °C since it is known that the temperature decays at increasing radial distances. Similar boundary conditions have been used in [17] and [19]. As concerns the brain-tissue thermal characteristics, the following values have been assumed: $\rho = 1000$ kg/m^3, $C = 3700$ J/(kg · °C), $K = 0.57$ W/(m · °C), $B = 40\,000$ W/(m^3 · °C) [30].

Fig. 4 shows, for a radiated power of 1.0 W, the time behavior of the temperature in a point placed at a radial distance of 3 mm from the antenna axis at the level of the first slot. The temperature reaches steady state following an exponential behavior with a time constant of approximately 60 s. Also in Fig. 4, the time behavior, obtained by using an explicit solution of the bioheat equation, previously developed by Bernardi *et al.* [30], is also reported. This figure shows a good agreement between the two formulations. Since the explicit formulation has been widely tested [30]–[32], this result validates the implemented ADI formulation.

It is noteworthy that the temporal step used in the ADI formulation is 10 s, while the stability criterion of the explicit formulation imposes a time step of 87.6 ms, which is approximately 100 times lower. Since the computer time necessary for computing a time step on a workstation equipped with a 2-GHz Pentium IV Xeon processor is approximately 1.6 s for the explicit formulation and 8 s for the ADI one, the overall time saving of the ADI can be quantified in a factor of approximately 20.

Fig. 5 shows the temperature distribution for 1.0 W of radiated power on the same plane of Fig. 3. Contour lines at $\Delta T = 6\,°\text{C}, 4\,°\text{C}$, and $2\,°\text{C}$ are drawn in this figure. In particular, the contour line at $\Delta T = 6$ °C encloses the region where the hyperthermia therapy is effective. The enclosed region is located around the antenna tip and, for the considered radiated power, this domain has maximum radial and longitudinal dimensions of approximately 6 and 12 mm, respectively. If the input power is increased to 2.0 W, the maximum dimensions of the therapeutic region increase to approximately 10×20 mm.

After considering the single antenna, arrays made of three identical antennas placed at the vertices of equilateral triangles of 10-, 15-, and 20-mm sides, respectively, have been studied. The ratio between the magnitude of reflected and incident waves, evaluated at the excitation section when all the three antennas are equally fed, is the same for the three antennas of each array, and is equal to 0.55, 0.52, and 0.48 for the 10-, 15-, and 20-mm cases, respectively [29]. These results show that increasing the distance among the antennas, the radiation impedance of each antenna of the array approaches the one of the single antenna.

Fig. 6(a)–(c) shows, for the three array configurations, the SAR contour plot over a horizontal section passing through the first antenna slot for a total radiated power of 1.0 W. This figure shows that the power deposition is mainly concentrated in the region among the antennas. The shape of the high absorption region is strongly dependent on the antenna spacing, while a fast decay is always evident in the array external region [29].

In order to provide some clinical indications about the optimal geometry and input power for achieving an efficient tumor heating, in this paper, the three considered array geometries have also been studied from the thermal point-of-view by varying the

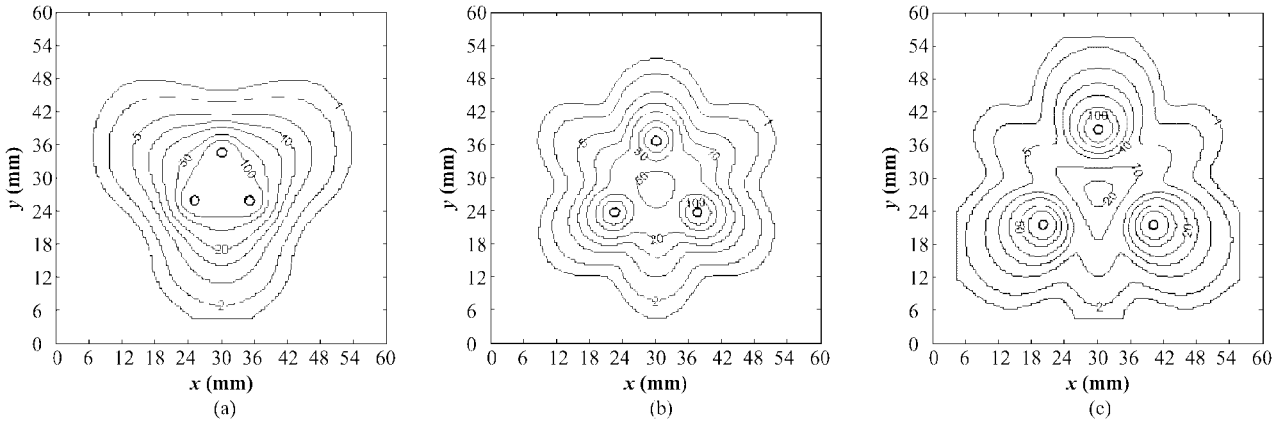

Fig. 6. SAR contour plot on a horizontal plane passing through the antenna slot for 1.0 W of radiated power and for: (a) 10-, (b) 15-, and (c) 20-mm array spacing. Contour levels are in watts per kilogram.

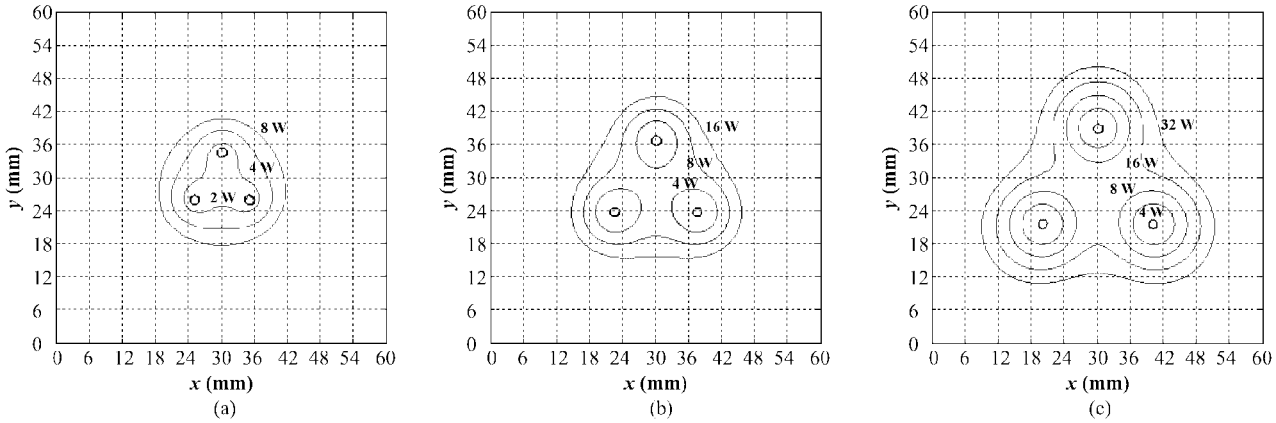

Fig. 7. Contour plot at $\Delta T = 6\,^{\circ}\mathrm{C}$ on a horizontal plane passing through the antenna slot for various radiated powers and for: (a) 10-, (b) 15-, and (c) 20-mm array spacing.

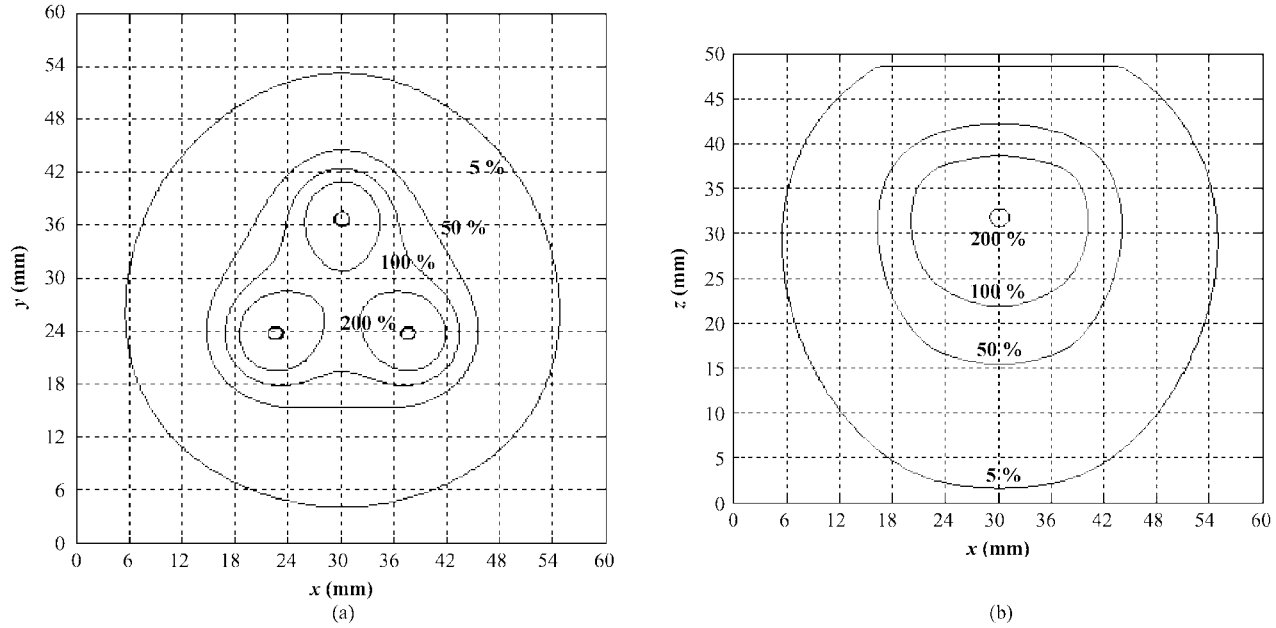

Fig. 8. Contour plot at $\Delta T = 6\,^{\circ}\mathrm{C}$: (a) on a horizontal plane passing through the antenna slot and (b) on a xz-vertical plane passing through the array center for different blood-perfusion values and for 8 W of input power, 15-mm array spacing.

input power. Fig. 7 shows the $\Delta T = 6\,^{\circ}\mathrm{C}$ contour line on a horizontal plane passing through the antenna slot for various input powers for the three considered array spacings. For each array spacing, there is a minimum input power below which the region above 43 °C is actually constituted by three regions around the three antennas. Once this power is exceeded, a simply connected domain is obtained. Moreover, the reported analysis evidences that, supposing a quasi-spherical tumor shape, for each tumor radius there is an optimal choice of the array spacing and input power. Finally, it can be observed that, for a tumor radius exceeding 20 mm, arrays made of more than three antennas become necessary.

It is well known that blood flow in the necrotic core of tumor tissues is remarkably low compared to normal tissue. Moreover, the rate of blood flow in normal tissue increases during hyperthermia. The effect of these variations has been investigated for the 15-mm spacing array by varying the B parameter in (2) from 5% to 200% of the nominal value. The 15-mm array spacing has been chosen since, as reported in [13] and [29], it produces the most uniform SAR distribution inside the array. The $\Delta T = 6\,^{\circ}\mathrm{C}$ contour lines in a horizontal plane passing through the first antenna slot and in the vertical xz-plane passing through the array center are shown in Fig. 8(a) and (b), respectively. The curves are plotted for different B values and for a fixed input power of 8 W. This figure demonstrates that the heat removal mechanism becomes less efficient as the blood flow is decreased. As a consequence, the effective region of hyperthermia therapy is enlarged. On the basis of this analysis, the reduced blood flow in the necrotic core and the blood flow increase in normal tissue are an aid to the hyperthermic therapy. In fact, the necrotic core region can be heated over 43 °C with less power and, in the external tumor region, the temperature decays quickly to 37 °C.

V. Conclusions

In this paper, a graded-mesh FDTD computer code, together with a 3-D ADI-FD solution of the bioheat equation, have been used to study both single antennas and arrays of miniature sleeved-slot antennas imbedded in a brain-equivalent phantom. The ability of these sleeved-slot antennas in heating deep-seated tumors without damaging superficial tissues has been demonstrated. Due to the high rate of brain blood perfusion, the heating is very fast, reaching a steady state in approximately 3 min. Our results indicate that deep-seated tumors, from 10 to 40 mm in diameter, can be treated by using equilateral triangular arrays of 10-, 15-, and 20-mm spacing for input powers that range from 2 to 32 W. Also, the results show that by taking into consideration a 50% reduction in blood perfusion rate—typical in the core of large tumors—the region where temperature is above 43 °C enlarges for a given input power of approximately 40%.

References

[1] B. Stea, J. Kittleson, and J. R. Cassady, "Treatment of malignant glioma with interstitial irradiation and hyperthermia," *Int. J. Radiat. Oncol. Biol. Phys.*, vol. 24, pp. 657–667, 1992.

[2] J. Overgaard, D. G. Gonzalez, M. C. C. M. Hulshof, G. Arcangeli, O. Dahl, O. Mella, and S. M. Bentzen, "Randomised trial of hyperthermia as adjuvant to radiotherapy for recurrent or metastatic malignant melanoma," *Lancet*, vol. 345, pp. 540–543, 1995.

[3] H. Kuwano, K. Sumiyoshi, M. Watanabe, N. Sadanaga, T. Nozoe, M. Yasuda, and K. Sugimachi, "Preoperative hyperthermia combined with chemotherapy and irradiation for the treatment of patients with esophageal carcinoma," *Tumori—J. Experimental and Clinical Oncol.*, vol. 81, pp. 18–22, 1995.

[4] T. Nakajima, D. W. Roberts, T. P. Ryan, P. J. Hoopes, C. T. Coughlin, B. S. Trembly, and J. W. Strohbehn, "Pattern of response to interstitial hyperthermia and brachytherapy for malignant intracranial tumour: A CT analysis," *Int. J. Hyperthermia*, vol. 9, pp. 491–502, 1993.

[5] P. K. Sneed, P. R. Stauffer, M. W. McDermott, C. J. Diederich, K. R. Lamborn, M. D. Prados, S. Chang, K. A. Weaver, L. Spry, M. K. Malec, S. A. Lamb, B. Voss, R. L. Davis, W. M. Wara, D. A. Larson, T. L. Phillips, and P. H. Gutin, "Survival benefit of hyperthermia in a prospective randomized trial of brachytherapy boost $+/-$ hyperthermia for glioblastoma multiforme," *Int. J. Radiat. Oncol. Biol. Phys.*, vol. 40, pp. 287–295, 1998.

[6] C. T. Coughlin, E. B. Douple, J. W. Strohbehn, J. W. Eaton, Jr., B. S. Trembly, and T. Z. Wong, "Interstitial hyperthermia in combination with brachytherapy," *Radiobiology*, vol. 148, pp. 285–288, 1983.

[7] R. W. P. King, B. S. Trembly, and J. W. Strohbehn, "The electromagnetic field of an insulated antenna in a conducting or dielectric medium," *IEEE Trans. Microwave Theory Tech.*, vol. MTT-31, pp. 574–583, July 1983.

[8] K. M. Jones, J. A. Mechling, B. S. Trembly, and J. W. Strohbehn, "SAR distribution for 915 MHz interstitial microwave antennas used in hyperthermia for cancer therapy," *IEEE Trans. Biomed. Eng.*, vol. 35, pp. 851–857, Oct. 1988.

[9] M. F. Iskander and A. M. Tumeh, "Design optimization of interstitial antennas," *IEEE Trans. Biomed. Eng.*, vol. 36, pp. 238–246, Feb. 1989.

[10] J. C. Lin and Y. J. Wang, "Interstitial microwave antennas for thermal therapy," *Int. J. Hyperthermia*, vol. 3, pp. 37–47, 1987.

[11] S. Pisa, M. Cavagnaro, P. Bernardi, and J. C. Lin, "A 915-MHz antenna for microwave thermal ablation treatment: Physical design, computer modeling and experimental measurement," *IEEE Trans. Biomed. Eng.*, vol. 48, pp. 599–601, May 2001.

[12] K. M. Jones, J. A. Mechling, J. W. Strohbehn, and B. S. Trembly, "Theoretical and experimental SAR distributions for interstitial dipole antenna arrays used in hyperthermia," *IEEE Trans. Microwave Theory Tech.*, vol. 37, pp. 1200–1208, Aug. 1989.

[13] J. C. Lin, S. Hirai, C. L. Chiang, W. L. Hsu, and Y. J. Wang, "Computer simulation and experimental studies of SAR distributions of interstitial arrays of sleeved-slot microwave antennas for hyperthermia treatment of brain tumors," *IEEE Trans. Microwave Theory Tech.*, vol. 48, pp. 2191–2197, Nov. 2000.

[14] J. C. Camart, J. J. Fabre, B. Prevost, J. Pribetich, and M. Chive, "Coaxial antenna array for 915 MHz interstitial hyperthermia: Design and modelization—power deposition and heating pattern—phased array," *IEEE Trans. Microwave Theory Tech.*, vol. 40, pp. 2243–2250, Dec. 1992.

[15] P. C. Cherry and M. F. Iskander, "FDTD analysis of power deposition patterns of an array of interstitial antennas for use in microwave hyperthermia," *IEEE Trans. Microwave Theory Tech.*, vol. 40, pp. 1692–1700, Aug. 1992.

[16] ——, "Calculations of heating patterns of an array of microwave interstitial antennas," *IEEE Trans. Biomed. Eng.*, vol. 40, pp. 771–779, Aug. 1993.

[17] G. B. Gentili, M. L. Leoncini, B. S. Trembly, and S. F. Schweizer, "FDTD electromagnetic and thermal analysis of interstitial hyperthermic applicators," *IEEE Trans. Biomed. Eng.*, vol. 42, pp. 973–980, Oct. 1995.

[18] O. P. Gandhi, Q. X. Li, and G. Kang, "Temperature rise for the human head for cellular telephones and for peak SAR's prescribed in safety guidelines," *IEEE Trans. Microwave Theory Tech.*, vol. 49, pp. 1607–1613, Sept. 2001.

[19] J. W. Strohbehn, B. S. Trembly, and E. B. Douple, "Blood flow effects on the temperature distributions from an invasive microwave antenna array used in cancer therapy," *IEEE Trans. Biomed. Eng.*, vol. BME-29, pp. 649–661, Sept. 1982.

[20] P. Bernardi, M. Cavagnaro, S. Pisa, and E. Piuzzi, "A graded-mesh FDTD code for the study of human exposure to cellular phones equipped with helical antennas," *ACES J.*, vol. 16, pp. 90–96, July 2001.

[21] M. N. O. Sadiku, *Numerical Techniques in Electromagnetics*. London, U.K.: CRC, 2001.
[22] A. Taflove and S. C. Hagness, *Computational Electrodynamics: The Finite-Difference Time-Domain Method*. Boston, MA: Artech House, 2000.
[23] S. D. Gedney, "An anisotropic perfectly matched layer-absorbing medium for the truncation of FDTD lattices," *IEEE Trans. Antennas Propagat.*, vol. 44, pp. 1630–1639, Dec. 1996.
[24] H. H. Pennes, "Analysis of tissue and arterial blood temperatures in resting forearm," *J. Appl. Physiol.*, vol. 1, pp. 93–122, 1948.
[25] R. G. Gordon, R. B. Roemer, and S. M. Horvath, "A mathematical model of the human temperature regulatory system—Transient cold exposure response," *IEEE Trans. Biomed. Eng.*, vol. BME-23, pp. 434–444, Nov. 1976.
[26] N. Ozisik, *Heat Transfer: A Basic Approach*. New York: McGraw-Hill, 1985.
[27] D. W. Peaceman and H. Rachford, "The numerical solution of parabolic and elliptic differential equations," *J. Soc. Ind. Applicat. Math.*, vol. 3, pp. 28–41, 1955.
[28] J. Douglas, "On the numerical integration of $u_{xx}+u_{yy}=u_t$ by implicit methods," *J. Soc. Ind. Applicat. Math.*, vol. 3, pp. 42–65, 1955.
[29] P. Bernardi, M. Cavagnaro, J. C. Lin, S. Pisa, and E. Piuzzi, "FDTD simulation of interstitial arrays of sleeved-slot antennas for hyperthermic cancer therapy," in *IEEE MTT-S Int. Microwave Symp. Dig.*, June 2003, pp. 395–398.
[30] P. Bernardi, M. Cavagnaro, S. Pisa, and E. Piuzzi, "Specific absorption rate and temperature elevation in a subject exposed in the far-field of radio-frequency sources operating in the 10–900-MHz range," *IEEE Trans. Biomed. Eng.*, vol. 50, pp. 295–304, Mar. 2003.
[31] ——, "SAR distribution and temperature increase in an anatomical model of the human eye exposed to the field radiated by the user antenna in a wireless LAN," *IEEE Trans. Microwave Theory Tech.*, vol. 46, pp. 2074–2082, Dec. 1998.
[32] ——, "Specific absorption rate and temperature increases in the head of a cellular phone user," *IEEE Trans. Microwave Theory Tech.*, vol. 48, pp. 1118–1126, July 2000.

Stefano Pisa (M'91) was born in Rome, Italy, in 1957. He received the Electronic Engineering and Ph.D. degrees from the University of Rome "La Sapienza," Rome, Italy, in 1985 and 1988, respectively.

In 1989, he joined the Department of Electronic Engineering, University "La Sapienza," as a Researcher. Since 2001, he has been an Associate Professor with the same university. His research interests are the interaction between EM fields and biological systems, therapeutic and diagnostic applications of EM fields, and the modeling and design of microwave circuits.

Dr. Pisa was the editor of the Disk of Complete References 1993–1995 for the Commission K (Electromagnetics in Biology and Medicine) of the International Union of Radio Science (URSI), published at the 25th URSI General Assembly. From 1995 to 1996, he was the coordinator of a "working package" on "Electromagnetic Environment Impact and Safety Issues" of the Italian project on "Wide Band Wireless Local Area Networks—WWLAN" of the Italian Research Council (CNR). From 1995 to 1999, he was a member of the Joint Working Group (JWG) 15 on "Measurement Techniques and Procedures for High-Frequency EM Fields With Regard to Human Exposure in the Frequency Range 10 kHz–300 GHz" created by International Electrotechnical Commission (IEC). From 1997 to 1999, he was the coordinator of the working package "Survey on Existing Dosimetric Work and Development of a Database" in the framework of the European project "Cellular Phones Standard" (CEPHOS). From 1995 to 2002, he was secretary of the IEEE Microwave Theory and Techniques Society (MTT-S)/Antennas and Propagation Society (AP-S) Central and South Italy Section Joint Chapter. He is currently the coordinator of the activity "Development and Optimization of Dedicated Software for the Evaluation of SAR in Subjects Exposed to Mobile Telecommunication Systems" of the Italian National Project (2001–2004) funded by the Ministry for Education, University, and Research, and was devoted to the protection of people and environment from EM emissions.

Marta Cavagnaro (M'01) was born in Rome, Italy, in 1966. She received the Electronic Engineering (*cum laude*) and Ph.D. degrees from the University of Rome "La Sapienza," Rome, Italy, in 1993 and 1997, respectively.

She is currently with the Department of Electronic Engineering, University of Rome "La Sapienza," as an Assistant Professor. Her current research interests are dosimetric aspects of the interaction between EM fields and biological systems and numerical techniques.

Dr. Cavagnaro was the recipient of the 1996 International Union of Radio Science (URSI) Young Scientist Award.

Emanuele Piuzzi was born in Galatina, Lecce, Italy, in 1972. He received the Electronic Engineering (*cum laude*) and Ph.D. degrees from the University of Rome "La Sapienza," Rome, Italy, in 1997 and 2001, respectively.

He is currently with the Department of Electronic Engineering, University of Rome "La Sapienza." His main research interests are related to the study of the interaction between EM fields radiated by mobile communication systems and exposed subjects and of therapeutic applications of EM fields (microwave tissue ablation and hyperthermic cancer treatment). He is currently studying smart antennas for cellular base stations.

Dr. Piuzzi was the recipient of one of the 1999 International Scientific Radio Union (URSI) Young Scientist Awards. He is currently the recipient of a University of Rome "La Sapienza," research fellowship.

Paolo Bernardi (M'66–SM'73–F'93–LF'01) was born in Civitavecchia, Italy, in 1936. He received the Electrical Engineering and Libera Docenza degrees from the University of Rome, Rome, Italy, in 1960 and 1968, respectively.

Since 1961, he has been with the Department of Electronics, University of Rome "La Sapienza," Rome, Italy, where he became a Full Professor in 1976 and served as Head of the Department from 1982 to 1988. He has authored over 180 scientific papers and numerous invited presentations at international workshops and conferences. His research has dealt with the propagation of EM waves in ferrites, microwave components, biological effects of EM waves, and EM compatibility. He is currently on the Editorial Board for *Microwave and Optical Technology Letters*. He was an Associate Editor for the *URSI Radio Science Bulletin*. He was the Guest Editor of special issues on "Nonionizing Electromagnetic Radiation" of *Alta Frequenza* (March 1980) and "Exposure Hazards and Health Protection in Personal Communication Services" of *Wireless Networks* (December 1997).

Dr. Bernardi is a member of the Bioelectromagnetics Society (BEMS), European Bioelectromagnetics Association (EBEA), and "Socio Fedele" of the Italian Electrical and Electronic Society (AEI). From 1979 to 1980, he was the chairman of the IEEE Middle and South Italy Section. He was chairman of the International Union of Radio Science (URSI) Commission K on Electromagnetics in Biology and Medicine (1993–1996), vice-chairman of the European Community COST Project 244 on Biomedical Effects of Electromagnetic Radiation (1993–1997), and project coordinator of the European Community Project CEPHOS (1998–2000), which was devoted to EM dosimetry and compliance with standards of mobile cellular phones. He is currently the scientific coordinator of the Italian National Project (2001–2004) devoted to the protection of people and environment from the EM emissions. He was an Editorial Board member for the IEEE TRANSACTIONS ON MICROWAVE THEORY AND TECHNIQUES. He was the recipient of the 1984 IEEE Centennial Medal.

James C. Lin (S'65–M'67–SM'77–F'86) received the B.S., M.S., and Ph.D. degrees in electrical engineering from the University of Washington, Seattle, in 1966, 1968, and 1971, respectively.

He is currently a Professor of electrical engineering and bioengineering at the University of Illinois at Chicago (UIC), where he has served as Director of the Robotics and Automation Laboratory, Head of the Bioengineering Department, and Director of Special Projects for the College of Engineering. He has authored or edited seven books and has authored 140 journal papers and book chapters. He has served as Editor and member of the Editorial Board of several journals, and as a columnist for four professional magazines. His current research interests include biomedical imaging and sensing, EM engineering for biology and medicine, minimally invasive technology for medical interventions, mobile telecommunication safety, biomedical instrumentation, biological interactions of EM radiation including RF, microwaves, and lasers, and telemedicine. He is listed in *American Men and Women of Science*, *Who's Who in America*, *Who's Who in Engineering*, *Who's Who in the World*, and *Men of Achievement.*

Dr. Lin is a Fellow of the American Association for the Advancement of Science (AAAS) and AIMBE. He is a member of Sigma Xi, Phi Tau Phi, Tau Beta Pi, and Golden Key honorary societies. He is an IEEE-EMBS distinguished lecturer. He held an NSC Research Chair from 1993 to 1997. He has served in leadership positions for several scientific and professional organizations including president of the Bioelectromagnetics Society, president of the Chinese American Academic and Professional Convention, president of Phi Tau Phi in Mid America, president of the Chinese Academic and Professional Association in Mid America, chairman of the International Scientific Radio Union (URSI) Commission on Electromagnetics in Biology and Medicine, chairman of the IEEE Committee on Man and Radiation, and chairman of NCRP Scientific Committee on Biological Effects and Exposure Criteria for Radiofrequency Fields. He has served on numerous advisory committees and panels for the Office of the U.S. President, National Academy of Sciences, National Research Council, National Science Foundation, National Institutes of Health, Marconi Foundation (Italy), Whitaker Foundation, the World Health Organization, and the U.S. Congress. He has given seminars to numerous universities in North America, Europe, and Asia, for example, Dartmouth University, The University of Michigan at Ann Arbor, the University of California at Los Angeles (UCLA), the University of Illinois at Urbana-Champaign (UIUC), the University of Tokyo, Tokyo, Japan, the University of Tsinghua, Beijing, China, National Taiwan University, Taiwan, R.O.C., The University of Rome "La Sapienza," Rome, Italy, the University of Manchester, Manchester, U.K., and the University of Waterloo, Waterloo, ON, Canada. He has served as chairman of several international conferences and workshops. He has been the recipient of numerous professional and scientific awards and recognitions, including the d'Arsonval Medal from the Bioelectromagnetics Society, the IEEE Electromagnetic Compatibility Transactions Prize Paper Award, the IEEE COMAR Recognition Award, the CAPAMA Outstanding Leadership and Service Awards, and the UIC Best Advisor Award.